

Fibroblast-Derived IL33 Facilitates Breast Cancer Metastasis by Modifying the Immune Microenvironment and Driving Type 2 Immunity



Ophir Shani¹, Tatiana Vorobyov¹, Lea Monteran¹, Dor Lavie¹, Noam Cohen¹, Yael Raz¹, Galia Tsarfaty², Camila Avivi³, Iris Barshack³, and Neta Erez¹

ABSTRACT

Lungs are one of the main sites of breast cancer metastasis. The metastatic microenvironment is essential to facilitate growth of disseminated tumor cells. Cancer-associated fibroblasts (CAF) are prominent players in the microenvironment of breast cancer. However, their role in the formation of a permissive metastatic niche is unresolved. Here we show that IL33 is upregulated in metastases-associated fibroblasts in mouse models of spontaneous breast cancer metastasis and in patients with breast cancer with lung metastasis. Upregulation of IL33 instigated type 2 inflammation in the metastatic microenvironment and mediated recruitment of eosinophils, neutrophils, and inflammatory monocytes to lung metastases. Importantly, targeting of IL33 *in vivo* resulted in

inhibition of lung metastasis and significant attenuation of immune cell recruitment and type 2 immunity. These findings demonstrate a key function of IL33 in facilitating lung metastatic relapse by modulating the immune microenvironment. Our study shows a novel interaction axis between CAF and immune cells and reveals the central role of CAF in establishing a hospitable inflammatory niche in lung metastasis.

Significance: This study elucidates a novel role for fibroblast-derived IL33 in facilitating breast cancer lung metastasis by modifying the immune microenvironment at the metastatic niche toward type 2 inflammation.

Introduction

Mortality from breast cancer is almost exclusively a result of tumor metastasis to distant organs. Advanced metastatic cancers are mostly incurable and available therapies only prolong life to a limited extent. It has become clear in recent years that the metastatic microenvironment plays a crucial role in enabling the growth of disseminated tumor cells (1). Changes in the metastatic niche precede metastases formation, and drive the formation of a hospitable microenvironment in multiple organs, mediated by modifications of the immune milieu and of the extracellular matrix (2).

Lungs are one of the most common sites of breast cancer metastasis. Various immune cell populations were shown to be functionally important in facilitating breast cancer pulmonary metastasis (3–6). Specifically, instigation of type 2 immunity was shown to be associated with pulmonary metastasis in multiple cancer types (7, 8). However, the mechanisms underlying these changes in the lung metastatic niche are largely unresolved.

IL33 is a member of the IL1 family of cytokines (9). It belongs to a group of alarmin molecules and its release from cells during cell injury instigates an inflammatory tissue damage response (10, 11). Under

physiologic conditions, IL33 is constitutively expressed in epithelial, endothelial, and fibroblastic cells, and is found in the nucleus (12, 13). During inflammation or other types of stress, IL33 is upregulated and released from necrotic or damaged cells (11). IL33 is an inducer of type 2 immune responses, implicated in multiple pathologies including allergic, fibrotic, infectious, and chronic inflammatory diseases (14). In lungs, IL33 was shown to be involved in mediating Th2 immune responses in models of allergic asthma (15, 16). In cancer, IL33 was demonstrated to have tumor-promoting as well as tumor-inhibiting functions in several tumor types (17). However, the role of IL33 in the context of the metastatic niche is largely unknown.

Cancer-associated fibroblasts (CAF) are a heterogeneous population of stromal cells in the microenvironment of solid tumors. In some cancer types, including breast carcinomas, CAFs are the most prominent stromal cell type, and their abundance correlates with worse prognosis (18). We previously demonstrated a novel role for CAFs in mediating tumor-promoting inflammation in mouse and human carcinomas (19–21). Importantly, there were profound changes in the expression of proinflammatory genes in fibroblasts isolated from metastases-bearing lungs (22, 23). However, very little is known about the role of fibroblasts during the complex process of metastases formation, and their interactions with immune cells in the metastatic microenvironment.

Here we show that IL33 is upregulated in the lung metastatic microenvironment, and that CAFs are the main cellular source of IL33 during breast cancer metastasis. Functionally, we found that stromal-derived IL33 drives type 2 inflammation and recruitment of multiple immune cell types to the lung microenvironment, which facilitated lung metastasis.

Materials and Methods

Mice

All experiments involving animals were approved by the Tel Aviv University Institutional Animal Care and Use Committee. MMTV-

¹Department of Pathology, Sackler Faculty of Medicine, Tel Aviv University, Tel Aviv, Israel. ²Department of Diagnostic Imaging, Chaim Sheba Medical Center, affiliated with Sackler Faculty of Medicine, Tel Aviv University, Tel Aviv, Israel. ³Department of Pathology, Sheba Medical Center, Tel Hashomer, affiliated with Sackler Faculty of Medicine, Tel Aviv University, Tel Aviv, Israel.

Note: Supplementary data for this article are available at Cancer Research Online (<http://cancerres.aacrjournals.org/>).

Corresponding Author: Neta Erez, Tel Aviv University, Sackler Faculty of Medicine, Tel Aviv, TA 69978, Israel. Phone: 9725-4490-0130; E-mail: netaerez@tauex.tau.ac.il

Cancer Res 2020;80:5317–29

doi: 10.1158/0008-5472.CAN-20-2116

©2020 American Association for Cancer Research.

Shani et al.

PyMT 634Mul/J transgenic mice were from Lisa Coussens. FVB/n; *Coll1a1*-YFP mice were a gift from Gustavo Leone. MMTV-PyMT were crossed with FVB/n; *Coll1a1*-YFP mice to create MMTV-PyMT; *Coll1a1*-YFP double-transgenic mice as we described previously (22). BALB/c; *Coll1a1*-YFP were generated in our lab. Nontransgenic BALB/c mice were purchased from Harlan, Israel. All animals were maintained at the Tel Aviv University Specific Pathogen Free facility.

Cancer cell lines and primary lung fibroblasts

Met-1 cells were received from Jeffrey Pollard. 4T1 cells were received from Zvi Granot. Tumor cell culture and conditioned media (CM) preparation were performed as described previously (21). Cell lines were not authenticated in our laboratory. All cell lines were routinely tested for *Mycoplasma* using the EZ-PCR-Mycoplasma Test Kit (Biological Industries; 20-700-20). Primary lung fibroblasts were isolated from lungs of FVB/n or BALB/c mice following dissociation of lung tissue as described previously (21). All experiments were performed with low passage (p2-4) fibroblasts.

Lung homogenate supernatant

Lungs were perfused with 10 mL PBS, harvested, and placed in 70 μ m cell strainers in 50 mL tube containing RPMI1640 media. Lungs were homogenized using a syringe plunger, and centrifuged 5 minutes at 500 g. Supernatants were collected and filtered through 0.45 μ m filters.

Bronchoalveolar lavage fluid

Mice bearing lung metastases or normal controls were euthanized, and 3 \times 500 μ L of PBS was injected intratracheally and recollected into the syringe. Bronchoalveolar lavage fluid (BALF) was concentrated using Amicon Ultra-0.5 Centrifugal Filter Units with Ultracel-10 membrane (Merck Millipore, UFC501024).

ELISA

ELISA for IL33 in lung homogenate supernatant or in BALF was performed using Mouse IL33 Quantikine ELISA Kit (R&D Systems, M3300).

Bone marrow-derived neutrophils and monocyte isolation

Bone marrow (BM) cells were isolated from the femur and tibia of 10-weeks old mice. Neutrophils and monocytes were separated by density gradient centrifugation, using Histopaque 1119 or 1077 (11191 and 10771, Sigma-Aldrich).

T-cell isolation

Spleens were harvested from 10–12 weeks old mice, minced and dissociated. T cells were isolated using Pan T-Cell isolation kit II (130-095-130).

BM-derived eosinophil isolation

BM from 6 weeks old mice was loaded using Histopaque gradient (10831, Sigma-Aldrich) and low-density cells were collected for culture. Cells were cultured in Iscove's modified Dulbecco's medium (12440053, Gibco) supplemented with 10% FCS, 100 ng/mL recombinant SCF (250-03-50, Peprotech), and 100 ng/mL recombinant Flt3 (250-31L, PeproTech) for 4 days. Media were supplemented with 10 ng/mL recombinant IL5 (215-15, PeproTech) for 11 days, changing medium every other day. On day 14, eosinophil purity was analyzed by flow cytometry and cytochemistry. >85% was defined as acceptable purity. Differential quick staining was performed using KIT DIF STAIN (KALTEK SRL, 1526).

Migration assays

BM-derived neutrophils (5×10^5), monocytes (5×10^5), T cells (1×10^6), and eosinophils (5×10^5 cells) were placed at the upper chamber of 24-transwell membrane plates (Corning; CA-3415, CLS3421, or CA-3422). Migration assays were performed with 5 μ m pore (neutrophils), 8 μ m pore (monocytes), or 3 μ m pore transwell inserts (T cells and eosinophils). Lung homogenate supernatant from normal or metastases-bearing lungs was placed at the bottom chamber. Neutralizing anti-IL33 antibody (0.2 μ g/mL AF3626, R&D Systems) was added and migrated cells were counted by cell counter.

Immunostaining

Tissue sections

Lungs were injected intratracheally with 600 μ L optimal cutting temperature (OCT) compound (BN62550, Tissue-Tek), harvested, washed in PBS, and embedded in OCT on dry ice. Serial sections were obtained to ensure equal sampling of the examined specimens (8 μ m trimming).

Immunofluorescence

Staining was performed as described previously (21). Anti-mouse IL33 antibody (2 μ g/mL), anti-YFP antibody (0.5 μ g/mL, ab6556 abcam), RedX-conjugated secondary antibody (705-295-147, Jackson ImmunoResearch Laboratories) and 488-conjugated secondary antibody (A21206, Invitrogen) were used. Slides were visualized using Leica SP5 microscope. Brightness and contrast were adjusted equally in all images. Quantitative analyses were performed using ImageJ Software. Metastases-bearing lung quantification was divided to fields of view (FOV) without metastases (Mets adj.) and FOV with metastases (Mets).

Hematoxylin and eosin staining

Hematoxylin and eosin (H&E) staining was performed as described previously (21). Images were obtained using the Leica Aperio VERSA slide scanner.

Orthotopic tumor transplantations

Tumor cells (2×10^5 4T1 cells) were suspended in PBS and mixed 1:1 with Matrigel (BD Biosciences, 354230). A total of 100 μ L of cell mixture was injected into the right inguinal mammary glands of 8-weeks-old female BALB/c mice. Tumors were resected 3 weeks following the injection.

In vivo experiments

IL33 Inhibition in vivo

One day following tumor resection, mice were injected intraperitoneally with 5 μ g/mouse of anti-IL33 antibody, or with 5 μ g isotype control antibody (AB-108-C, R&D Systems). For eosinophil ablation, mice were injected with 15 μ g/mouse anti-SiglecF antibody (MAB17061, R&D Systems), or with 15 μ g/mouse isotype control (MAB006R, R&D Systems), alone or in combination with anti-IL33 as indicated in Supplementary Fig. S4. Injections were performed twice weekly to a total of five injections. Mice were euthanized one day after the last injection.

Quantification of lung metastatic load

CT imaging and quantification

CT imaging of lungs was performed one day after the last injection, prior to euthanizing the mice. Images were analyzed by a specialist radiologist. Metastasis quantification included counting the total number of metastases, and measurement of metastatic area and volume.

H&E quantification

Quantification of lung metastatic load was performed by analyzing the number of metastatic nodules per section or by evaluating the metastatic area per section normalized to lung area per section using ImageScope.

Human IL33 staining

Human patient samples were collected with written informed consent and processed at the Sheba Medical Center, Israel, in accordance with recognized ethical guidelines, under an approved Institutional Review Board (3112-16). Tissue sections stained for IL33 (AF3625, R&D Systems) were analyzed by an expert pathologist. Images were scanned at $\times 20$ magnification using the Leica Aperio VERSA slide scanner. Analysis was performed using ImageScope software. In each slide, 5–10 areas of metastases and 5–10 normal areas were arbitrarily selected and quantified for IL33⁺ cells.

FACS sorting

Single-cell suspensions of normal lungs and metastases-bearing lungs isolated from FVB/n; *Col1a1*-YFP, MMTV-PyMT; *Col1a1*-YFP or BALB/c; *Col1a1*-YFP mice were stained and isolated as described previously (22).

Flow cytometry analysis

Immune cell infiltration to lungs and ST2 analysis

Single-cell suspensions of normal lungs and metastases-bearing lungs were incubated with anti-mouse CD16/CD32 (eBioscience, 16-0161-82) for 15 minutes, followed by staining with the following anti-mouse antibodies: anti-CD45-BV650 (BioLegend, BLG-103151), anti-CD11b-PeCy7 (BioLegend, BLG-101216), anti-CD11c-PerCP-Cy5.5 (eBioscience, 45-0114), anti-SiglecF-APC-R700 (BD Biosciences, BD565183), anti-Ly6G-APC (BioLegend, 127614), anti-Ly6C-FITC (BioLegend, 128006), anti-NKp46-PeCy7 (BioLegend, BLG-137618), anti-B220-PerCP-Cy5.5 (BioLegend, BLG-103236), anti-CD4-APC-Cy7 (BioLegend, BLG-100413), anti-CD8a-APC (BioLegend, BLG-100712), anti-CD3-FITC (eBioscience, 11-0031), anti-ST2-PE (BioLegend, 145303), and DAPI (Molecular Probes; D3571). Specificity of staining was validated by appropriate isotype control per each antibody and by fluorescence minus one (FMO) method. Immune populations were defined on the basis of previous studies of lung immune populations (24, 25).

Eosinophil purity *in vitro*

Cultured BM cells were stained with anti-SiglecF-APC-R700 and anti-CCR3-FITC (eBioscience, FAB729F) and analyzed for eosinophil purity. Flow cytometric analyses were performed using CytoFLEX Flow Cytometer (Beckman Coulter). Data analysis was performed with the Kaluza Flow Analysis software (Beckman Coulter).

RNA isolation and qRT-PCR

RNA from sorted cells was isolated using the EZ-RNAl Kit (20-410-100, biological industries). RNA from *in vitro* experiments and from total lungs was isolated using the PureLink RNA Mini Kit (Invitrogen; 12183018A). cDNA synthesis was conducted using qScript cDNA Synthesis Kit (Quanta, 95047-100). qRT-PCR were conducted using PerfeCTa SYBR Green Fastmix ROX (Quanta, 95073-012). Expression results were normalized to *Gusb*, *Gapdh*, or *Ubc* and to controls. RQ ($2^{-\Delta\Delta C_t}$) was calculated.

RNA-seq analysis

Expression analysis of inflammatory genes was based on a dataset we described previously [GSE128999 (23)]. Gene Ontology (GO)-term

enrichment analysis was performed on genes overexpressed in metastases-associated fibroblasts (MAF) as compared with normal lung fibroblasts (fold change > 1.5, adjusted *P* value < 0.05) using the STRING platform. Heatmap was generated on the basis of gene expression Z-scored per gene derived from RNAseq data.

Human data

Stromal and epithelial expression of *IL33* were analyzed in human breast cancer based on a publicly available datasets GSE14548 (26), GSE9014, GSE12622 (27), and GSE88715 (28). Metastatic site expression of *IL33* were analyzed in human breast cancer based on a publicly available dataset GSE14020 (29, 30).

Statistical analysis

Statistical analyses were performed using GraphPad Prism software. All tests were two-tailed unless otherwise stated. Bar graphs represent mean and SD of at least three separate biological repeats. *P* value of ≤ 0.05 was considered statistically significant.

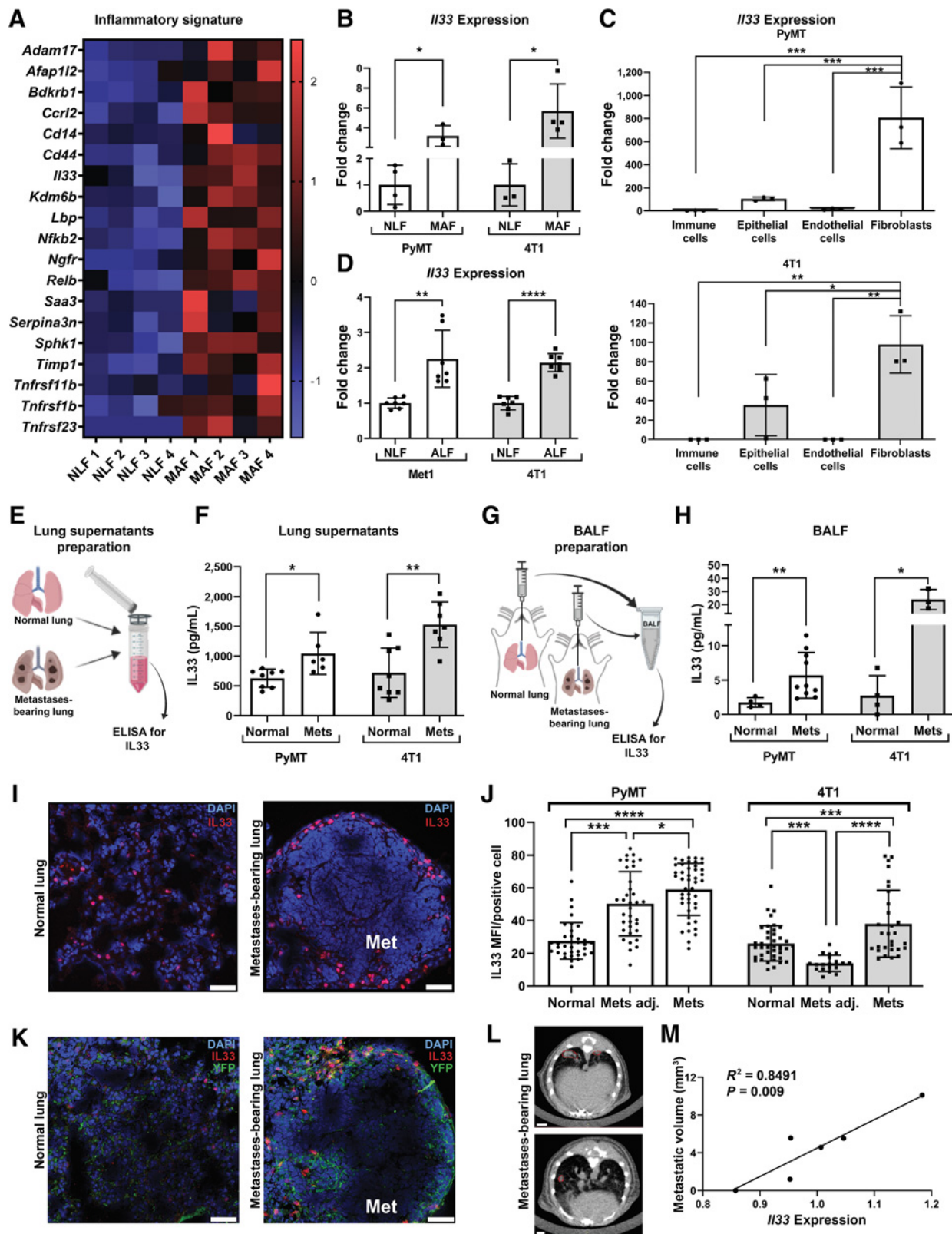
Results

IL33 is upregulated in MAFs at the lung metastatic microenvironment

We previously characterized the coevolution of MAFs in breast cancer lung metastases by profiling their transcriptome at distinct metastatic stages, using fibroblasts that were isolated from MMTV-PyMT; *Col1a1*-YFP transgenic mice, in which all fibroblasts are fluorescently labeled (23). Utilizing GO analysis, we found that an inflammatory gene signature was highly enriched in fibroblasts isolated from MAF in lung macrometastases as compared with normal lung fibroblasts (NLF; Fig. 1A). Specifically, analysis of the data revealed that one of the genes that were highly upregulated in MAF is *Il33*.

IL33 is a stromal cytokine with multiple known functions in both physiologic and pathophysiologic settings. While *IL33* was implicated in breast cancer (31, 32), very little is known regarding its role in the metastatic niche, and even less is known about its role in fibroblasts. Intrigued by this finding, we set out to validate the expression of *IL33* in fibroblasts isolated by FACS from spontaneous lung metastases in MMTV-PyMT mice, as well as in an additional mouse model of breast cancer metastasis to lungs, the transplantable 4T1 triple-negative tumor cells, orthotopically injected to BALB/c; *Col1a1*-YFP mice. The results confirmed that *IL33* is significantly upregulated in MAF (Fig. 1B). Because *IL33* is expressed by various cell types, we next assessed the cellular origin of *IL33* in the lung metastatic niche. To that end, we isolated by FACS immune cells (CD45⁺CD31⁻), endothelial cells (CD31⁺CD45⁻), epithelial/tumor cells (EpCAM⁺CD45⁻CD31⁻) or fibroblasts (YFP⁺CD45⁻CD31⁻EpCAM⁻) from metastases-bearing lungs (Supplementary Fig. S1A). Analysis of *Il33* expression indicated that fibroblasts exhibited the highest expression of *Il33* in both the autochthonous and the transplantable models, suggesting that fibroblasts are the main source of *Il33* in lung metastases (Fig. 1C). Of note, the basal expression of *Il33* was not altered in epithelial cells at the metastatic lung as compared with normal lung (Supplementary Fig. S1B). Interestingly, *in vitro* expression of *Il33* in NLFs was elevated in response to activation with the tumor cell-conditioned medium, suggesting that reprogramming by tumor cell-secreted factors may drive the upregulation of *IL33* in MAF (Fig. 1D). In addition to its intracellular roles, *IL33* functions as a proinflammatory/alarmin cytokine (33). To

Shani et al.



investigate whether secreted/extracellular IL33 is operative in the lung microenvironment, we analyzed IL33 in lung tissue supernatants of metastases-bearing lungs compared with normal lungs, and in the content of BALF from normal or metastases-bearing lungs. We found that protein levels of IL33 were significantly higher in BALF and lung supernatants isolated from metastases-bearing lungs compared with normal controls (Fig. 1E–H).

To further assess the expression of IL33 in the lung metastatic microenvironment, we performed immunofluorescent staining of IL33 in metastases-bearing lungs and in normal controls. While in normal lungs, there was sparse IL33 expression in lung parenchymal cells, IL33 was elevated in lungs of mice with metastases, particularly around metastatic lesions. Furthermore, the levels of expression per cell were the highest in stromal cells located within metastatic lesions, compared with cells in lung areas adjacent to metastases or in normal lungs (Fig. 1I and J; Supplementary Fig. S1C). Moreover, costaining of YFP⁺ fibroblasts and IL33 confirmed that IL33 is almost exclusively expressed by fibroblasts (Fig. 1K).

To test the functional importance of these findings, we next asked whether *Il33* expression is correlated with lung metastasis. Quantification of lung metastatic volume by CT imaging in 4T1 injected mice (Fig. 1L) and analysis of *Il33* expression in total lungs, revealed that *Il33* expression significantly correlated with metastatic load (Fig. 1M), implying that fibroblast-derived IL33 may be functionally important in metastatic progression. Taken together, these results indicate that the expression of IL33 is specifically upregulated in lung MAFs and suggest a role for stromal IL33 in the lung metastatic niche.

Lung metastases formation is characterized by extensive modifications in the immune milieu

Because tumor metastasis is accompanied by significant changes in the immune microenvironment and IL33 is a known immune modulator and a driver of type 2 immunity (10), we hypothesized that stromal upregulation of IL33 mediates changes in the metastatic immune microenvironment. To test this hypothesis, we initially analyzed the expression of multiple cytokines and chemokines that were implicated as *Il33* downstream genes (34), in metastases-bearing lungs or in normal lungs. Analysis of the results confirmed a significant upregulation in the expression of multiple immune-related genes (Fig. 2A; Supplementary Fig. S2A). In addition, because IL33 is known to mediate type 2 inflammation, we analyzed the expression of

transcription factors (TF) associated with type-1 (Tbet) and type 2 immunity (Gata3, Foxp3). We found in the 4T1 model, that while the expression of Gata3 and Foxp3 was unchanged, there was a significant downregulation in the expression of Tbet, a TF associated with type-1 immunity and with tumor rejection (Fig. 2B). Interestingly, in the transgenic PyMT model, Gata3 was significantly elevated while Tbet was unchanged (Supplementary Fig. S2B), suggesting that different modulations of gene expression are operative to drive transcriptional regulation toward type 2 immunity, in a context-dependent manner. Furthermore, there was a significant positive correlation between the expression of IL33 and the expression levels of many of the immune-related factors that we analyzed, and a negative correlation with the expression of Tbet (Fig. 2C), further implicating IL33 in modifying the immune microenvironment in lung metastasis.

To assess whether these changes in gene expression are reflected in modifications in the lung immune milieu, we characterized immune cell populations in the microenvironment of metastatic lungs compared with normal lungs. Analysis revealed that the number of immune cells was significantly increased in metastases-bearing lungs, pointing at the massive immune infiltration that accompanies metastases formation (Fig. 2D). To further characterize the immune milieu, we performed a comprehensive flow cytometry analysis in the lung metastatic microenvironment compared with normal controls. Analysis of the results showed significant changes in the composition of immune cell populations in metastases-bearing lungs, in both the transgenic and transplantable models (Fig. 2E; Supplementary Fig. S2C and S2D). Interestingly, some of the changes in immune cell populations were different between the mouse models: while in the 4T1 model, the most striking change was a massive increase in eosinophils, the most prominent change in the PYMT model was in the neutrophil population, suggesting that the specific composition of the immune cell milieu is dependent on the pathologic context (Fig. 2E and I). A detailed analysis of immune cell infiltration in the lung metastatic microenvironment revealed that while recruitment of eosinophils, B cells, CD8⁺ T cells, and dendritic cells was model specific, significant increases in the numbers of neutrophils, inflammatory monocytes, and CD4⁺ T cells were common to both models (Fig. 2F–J). These results reveal the substantial changes in immune cell infiltration and milieu at the metastatic lung, with a great increase in both number and fraction of eosinophils, neutrophils, and inflammatory monocytes, suggesting that these cells have a functional role in lung metastasis.

Figure 1.

IL33 is upregulated in MAFs at the lung metastatic microenvironment. **A**, Heatmap of inflammatory genes that were enriched in an unbiased GO analysis (GO:0006954, FDR = 0.00045). Analysis was performed on genes significantly upregulated in MAF versus NLF (FC > 1.5; adjusted $P < 0.05$). **B**, Expression of *Il33* in NLF and MAF sorted from MMTV-PyMT; *Col1a1*-YFP transgenic mice ($n = 3$) versus normal FVB/n; *Col1a1*-YFP controls ($n = 4$) and BALB/c; *Col1a1*-YFP mice bearing 4T1 metastases ($n = 4$) versus BALB/c; *Col1a1*-YFP controls ($n = 3$). Data are presented as fold change \pm SD. Welch t test. *, $P < 0.05$. **C**, qRT-PCR analysis of *Il33* expression in FACS sorted lung cell populations. Cells were isolated from MMTV-PyMT; *Col1a1*-YFP mice ($n = 3$) or BALB/c; *Col1a1*-YFP mice bearing 4T1 tumor cell metastases ($n = 3$). Data presented as mean \pm SD, normalized to control immune cells; one-way ANOVA followed by Tukey multiple comparisons test. *, $P < 0.05$; **, $P < 0.01$; ***, $P < 0.001$. **D**, qRT-PCR analysis of *Il33* expression. White bars, FVB/n lung fibroblasts incubated with SFM (NLF, $n = 7$) or with Met1 tumor cells CM (ALF-activated lung fibroblasts, $n = 6$). Gray bars, BALB/c NLF incubated with SFM ($n = 7$) or ALF ($n = 7$) incubated with 4T1 tumor cells CM. Data presented as mean \pm SD; Welch t test. **, $P < 0.01$; ****, $P < 0.0001$. **E**, Scheme of IL33 ELISA in lung homogenate supernatants. **F**, Quantification of IL33 ELISA presented in **E**: FVB/n normal lungs ($n = 7$) versus MMTV-PyMT metastases-bearing lungs (Mets; $n = 6$) and BALB/c normal lungs ($n = 8$) versus BALB/c mice bearing 4T1 metastases ($n = 7$). Data presented as mean \pm SD; Welch t test. *, $P < 0.05$; **, $P < 0.01$. **G**, Scheme of IL33 ELISA in BALF. **H**, Quantification of IL33 ELISA presented in **G**: FVB/n normal lungs ($n = 4$) versus MMTV-PyMT metastases-bearing lungs ($n = 10$) and BALB/c normal lungs ($n = 4$) versus BALB/c mice bearing 4T1 metastases ($n = 3$). Data presented as mean \pm SD. Welch t test. *, $P < 0.05$; **, $P < 0.01$. **I**, Representative images of IL33 immunofluorescence staining in lungs. $n = 3$ mice per group. Scale bars, 50 μ m. Cell nuclei, DAPI; IL33, Rhodamine Red. **J**, Quantification of mean fluorescent intensity (MFI) per IL33⁺-positive cell in staining performed in **I**. FVB/n normal lungs versus PyMT metastases-bearing lungs, and BALB/c normal lungs versus mice bearing 4T1 lung metastases. 6–8 FOV/lung were analyzed. Mets adj., lung areas without metastases; Mets, metastases. One-way ANOVA with Tukey correction for multiple comparisons. *, $P < 0.05$; **, $P < 0.01$; ***, $P < 0.001$; ****, $P < 0.0001$. **K**, Representative images of IL33 and YFP immunofluorescence staining in lungs. $n = 3$ mice per group. Scale bars, 50 μ m. Cell nuclei, DAPI; IL33, Rhodamine Red; YFP, Alexa Fluor-488. **L**, Representative CT imaging of 4T1 lung metastasis. Red, metastases. $n = 4$. **M**, Pearson correlation analysis between metastatic volume (mm³) measured by CT imaging presented in **L** and *Il33* expression analyzed by qRT-PCR in total lungs.

Shani et al.

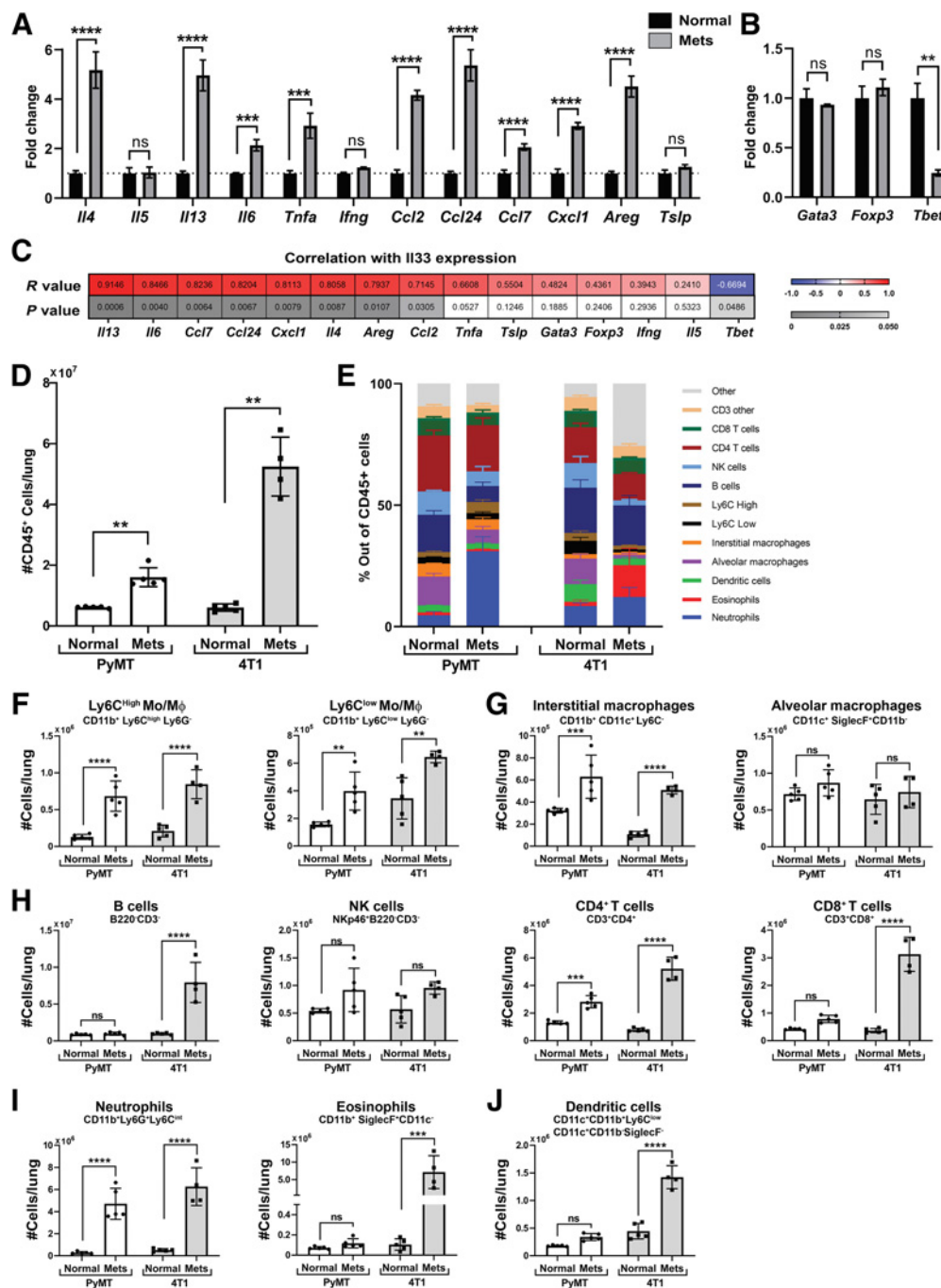


Figure 2.

Lung metastases formation is characterized by extensive modifications in the immune milieu. **A** and **B**, qRT-PCR analysis of *//33* downstream genes (**A**) and immune-related TFs (**B**) in total lungs derived from BALB/c mice bearing 4T1 tumor cell metastases ($n = 4$) and in normal controls ($n = 5$). Data are presented as mean \pm SD of technical repeats. Multiple t tests with Welch correction, FDR(Q) = 5%, and fold change >1.5 . **, $q < 0.01$; ***, $q < 0.001$; ****, $q < 0.0001$; ns, not significant. **C**, Heatmap presenting Pearson correlation analysis between *//33* expression and the expression of the genes presented in **A** and **B**. Results are presented as Pearson R values and P values per gene. Significant results were considered as $P < 0.05$ and $R > |0.65|$. **D**, Flow cytometry analysis of the number of immune cells in normal lungs and metastases-bearing lungs derived from FVB/n normal lungs (Normal; $n = 5$) versus MMTV-PyMT metastases-bearing lungs (Mets; $n = 5$) and BALB/c normal lungs ($n = 5$) versus BALB/c mice bearing 4T1 tumor cell metastases following orthotopic injection ($n = 4$). Data presented as mean \pm SD. Welch t test, **, $P < 0.01$. **E**, Quantification of flow cytometry analysis of immune cell populations in the lung derived from FVB/n normal lungs (Normal; $n = 5$) versus MMTV-PyMT metastases-bearing lungs (Mets; $n = 5$) and BALB/c normal lungs ($n = 5$) versus BALB/c mice bearing 4T1 tumor cell metastases following orthotopic injection ($n = 4$). Data presented as mean \pm SD of percent out of CD45⁺ cells. Gating strategy presented in Supplementary Fig. S2C and S2D. Cell numbers of different populations based on quantification performed in **E**, monocytes presented in **F**, macrophages presented in **G**, lymphoid cells presented in **H**, granulocytes presented in **I**, and dendritic cells in **J**. Two-way ANOVA with Sidak correction for multiple comparisons. **, $P < 0.01$; ***, $P < 0.001$; ****, $P < 0.0001$.

ST2, the IL33 receptor, is highly upregulated in immune cells at the metastatic microenvironment

To test whether stromal IL33 may affect these changes in the metastatic immune microenvironment, we next analyzed the expression and distribution of ST2, the receptor of IL33, on various cell populations in lungs. ST2 is known to be expressed by immune cells, but it was also shown to be expressed by stromal cells and tumor cells (35). We analyzed the expression of ST2 on various cell populations isolated by FACS from normal lungs, compared with cells isolated from metastases-bearing lungs of both the MMTV-PyMT transgenic model and the 4T1 transplantable model. We found that ST2 is expressed almost exclusively on CD45⁺ immune cells (Fig. 3A). Furthermore, the expression of ST2 was upregulated in immune cells isolated from metastases-bearing lungs as compared with normal lungs (Fig. 3A–D). To examine which immune cells express ST2, we assessed its expression on different immune subpopulations by flow cytometry analysis. Interestingly, upregulation of ST2 expression was highest on metastases-associated eosinophils, neutrophils, and inflammatory monocytes, which were the cell types most highly recruited into metastatic lungs (Fig. 3E–H). These results further supported our hypothesis that stromal-derived IL33 may affect the recruitment and/or function of immune cells in the lung metastatic microenvironment.

IL33 is functionally important for direct recruitment of T cells and eosinophils

To test whether IL33 is functional in recruitment of eosinophils, neutrophils, monocytes, and T cells, we analyzed *in vitro* the migration of these cells toward lung supernatants prepared from normal lungs, metastases-bearing lungs or metastases-bearing lungs supplemented with anti-IL33 (Fig. 4A). Notably, the migration of all the tested immune cell types was significantly enhanced in response to factors in metastases-bearing lungs compared with normal lungs (Fig. 4B–D and F). Interestingly, inhibiting the function of IL33 in supernatant from metastatic lungs, by adding anti-IL33 antibodies significantly inhibited the migration of T cells (Fig. 4D) and of eosinophils (Fig. 4E and F; Supplementary Fig. S3A and S3B), suggesting a direct role for IL33 in the recruitment of these cell populations to lungs. However, while there was a trend toward attenuation of migration, inhibition of IL33 did not significantly inhibit the migration of monocytes and neutrophils (Fig. 4B and C). This discrepancy may be explained by the fact that some of the IL33 downstream genes that were upregulated in metastatic lungs such as *Ccl2* and *Cxcl1* (Fig. 2A and C) are known chemoattractants for monocytes and neutrophils, and inhibition of IL33 *in vitro* did not abrogate their function in the lung supernatant. Taken together, these results suggest that MAF-derived IL33 mediates the recruitment of immune cells to the lung metastatic microenvironment.

Inhibition of IL33 attenuates lung metastases and tempers type 2 immunity in the metastatic lung

To elucidate the functional role of IL33 in lung metastasis *in vivo*, we performed experiments to inhibit IL33 in an adjuvant setting. The autochthonous growth of mammary tumors in the transgenic MMTV-PyMT mouse model is characterized by formation of multiple primary tumors that are nonresectable, and therefore do not mimic the clinical settings of breast cancer metastatic relapse. To recapitulate the clinical setting, we utilized for these experiments the 4T1 model of spontaneous lung metastasis following resection of a transplanted mammary tumor. Tumor cells were injected orthotopically to the mammary gland, and surgically resected after 3 weeks, when they reached a size of approximately 0.3 cm³. Following tumor resection, we treated mice

with anti-IL33 antibody or isotype control (Fig. 5A). Lung metastatic load was assessed intravitaly by CT imaging (Fig. 5B–D), followed by H&E staining of lung tissue sections (Fig. 5E–G). Analysis of the results revealed a striking decrease in the number of metastatic foci as well as in the size of metastatic lesions in mice treated with anti-IL33 antibody, implying that IL33 is functionally important in the formation of breast cancer lung metastasis.

Seeking to get mechanistic insight on the metastases-promoting function of IL33, and based on our findings that lung metastases are characterized by significant recruitment of immune cells and upregulation of ST2 expression and type 2 immunity, we next analyzed the immune cell composition in lungs of mice treated with anti-IL33 as compared with controls. We found that targeting IL33 *in vivo* resulted in a strong inhibition of immune cell recruitment to metastatic lungs (Fig. 5H).

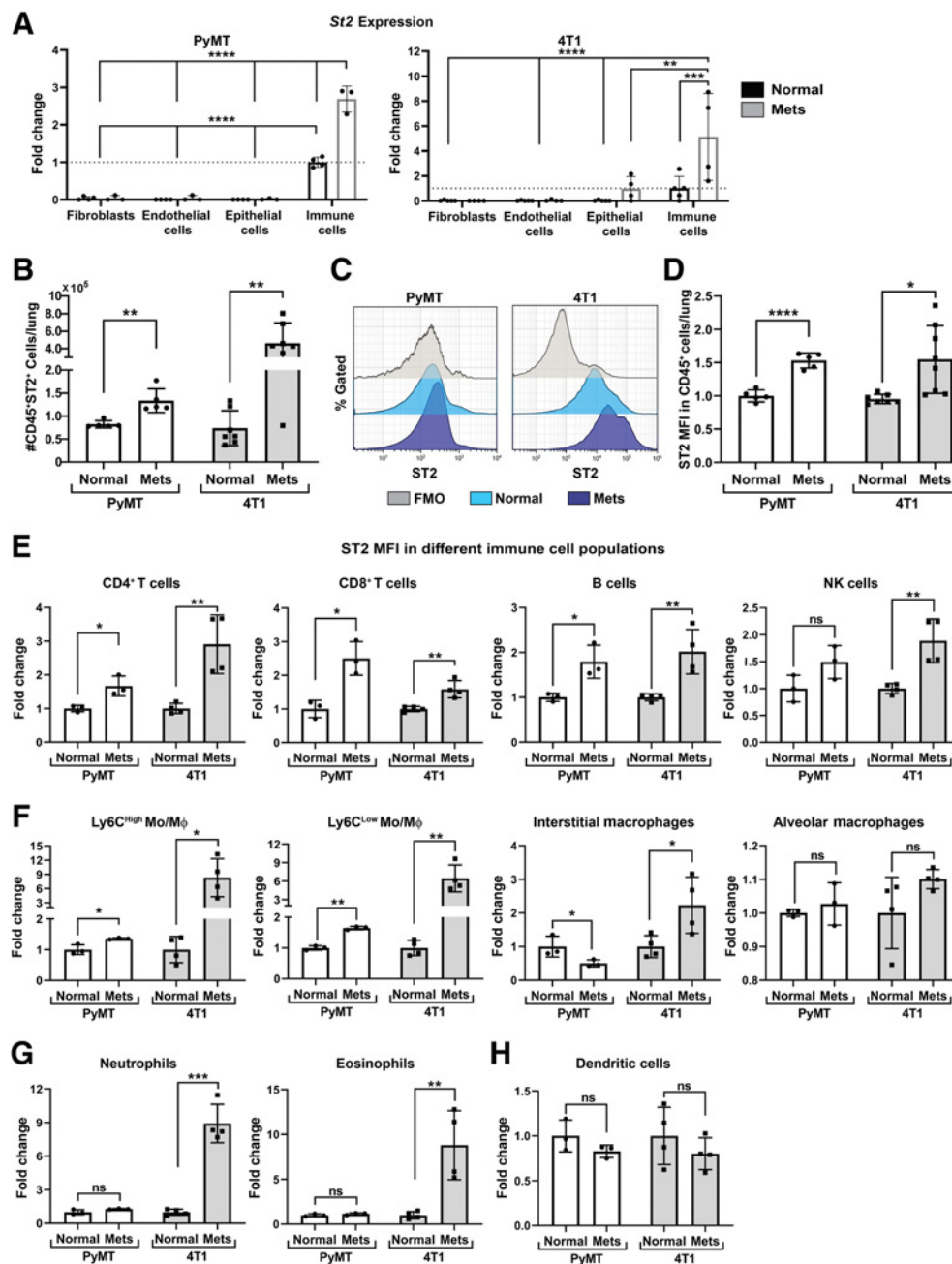
Because eosinophils were the most strikingly recruited population to lung metastases of 4T1-injected mice (Fig. 2E and I), and inhibition of IL33 attenuated their recruitment, we hypothesized that eosinophils may be functionally important downstream of IL33 in metastasis promotion. To test whether eosinophil ablation would mimic IL33 inhibition, 4T1-injected mice were treated following resection of the primary tumor with anti-SiglecF, to eliminate eosinophils, or with anti-IL33, or both (Supplementary Fig. S4A). Analysis of eosinophil presence in lungs revealed that inhibition of IL33 was comparable with anti-SiglecF treatment in reducing eosinophil infiltration to lungs, further confirming the essential role of IL33 in eosinophil recruitment *in vivo* (Supplementary Fig. S4B and S4C). However, analysis of metastatic burden revealed that inhibition of IL33 was more efficient in attenuating metastasis than eosinophil elimination (Supplementary Fig. S4D–S4F). Moreover, the combined treatment of anti-IL33 and anti-SiglecF had no additive effect on metastatic incidence or burden compared with the single treatment. These results suggest that the role of IL33 in promoting metastasis is pleiotropic, and is not eosinophil dependent.

To further assess the immune-modulating effect of IL33, we analyzed the expression of multiple IL33 downstream chemokines and cytokines, in lungs of mice treated with anti-IL33, and found that inhibition of IL33 resulted in a significant decrease in the expression of type 2 immunity related genes. We also analyzed the expression of IFN γ and TNF α , known to be related to type-1 immunity, and found that targeting IL33 did not affect their expression (Fig. 5I). Notably, *Cxcl1*, a known neutrophil chemoattractant, was unchanged by IL33 inhibition, in agreement with our finding that neutrophil infiltration to lungs was not affected by IL33 inhibition (Fig. 5H). Moreover, analysis of the expression of the TFs *Gata3*, *Foxp3*, and *Tbet* in response to IL33 inhibition revealed a significant attenuation of the expression of *Gata3*, known to regulate type 2 immune response, with no change in the expression of *Foxp3* or *Tbet* (Fig. 5J). Taken together, these findings functionally implicate IL33 in facilitating lung metastatic relapse and in mediating metastases-promoting type 2 immunity in lungs.

IL33 is upregulated in the stroma of breast cancer primary tumors and lung metastases in human patients

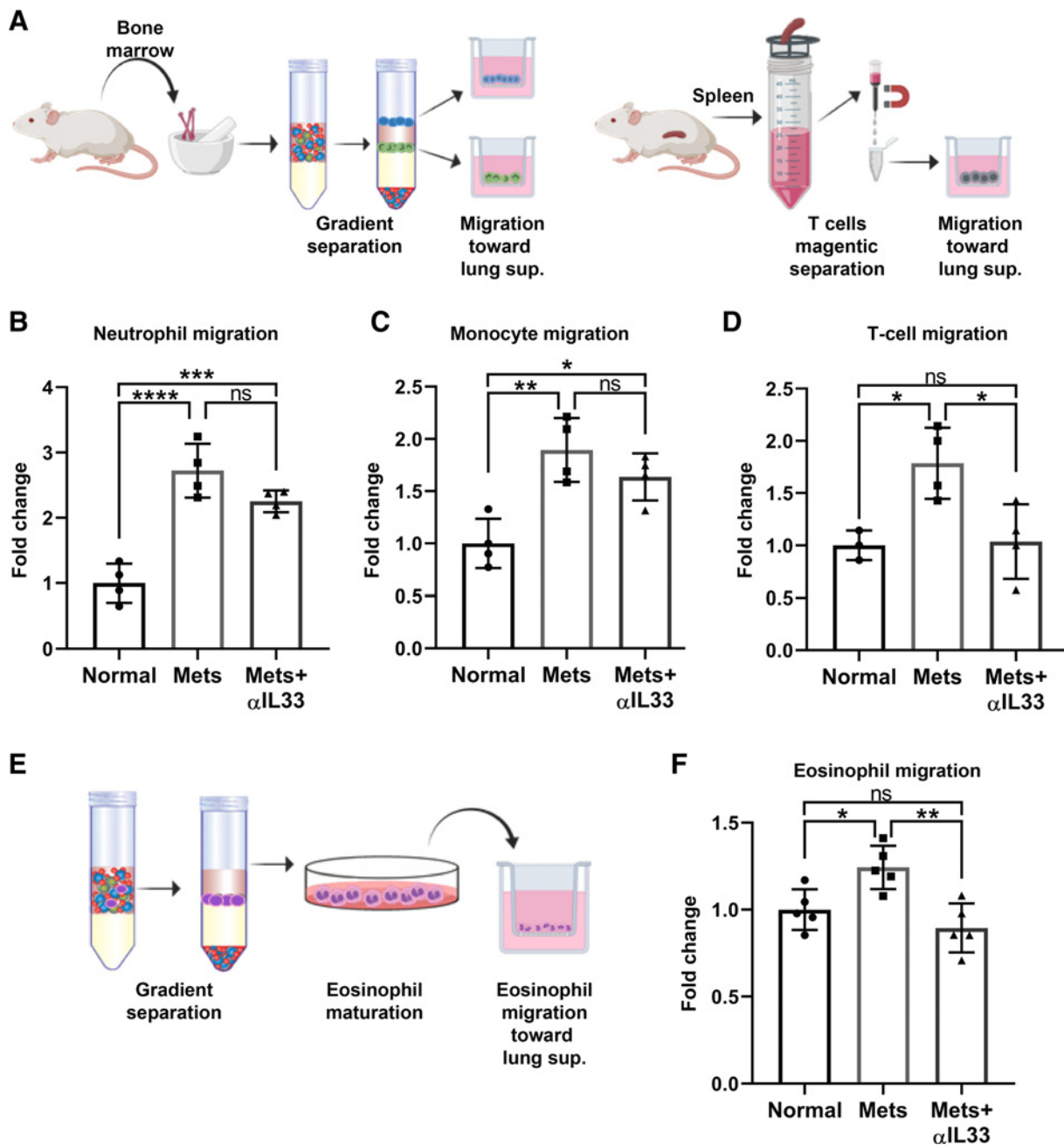
Finally, we asked whether upregulation of stromal IL33 is also operative in human primary breast cancer and lung metastasis. To address this question, we analyzed IL33 expression in human breast tumors from several datasets (26–28). Initially, we analyzed the expression of *IL33* in normal stroma compared with tumor-associated stroma and found that *IL33* is significantly upregulated in the stromal compartment (Fig. 6A). Moreover, analysis of IL33

Shani et al.

**Figure 3.**

ST2, the IL33 receptor, is highly upregulated in immune cells at the metastatic microenvironment. **A**, qRT-PCR analysis of *St2* expression in FACS sorted lung cell populations, immune cells ($CD45^+CD31^-$), endothelial cells ($CD31^+CD45^-$), epithelial/tumor cells ($EpCAM^+CD45^-CD31^-$), or fibroblasts ($YFP^+CD45^-CD31^-EpCAM^-$). Cells were sorted by flow cytometry from MMTV-PyMT;*Col1a1*-YFP mice ($n = 3$), FVB/*n*;*Col1a1*-YFP ($n = 4$), or BALB/*c*;*Col1a1*-YFP mice bearing 4T1 tumor cell metastases ($n = 4$) or normal BALB/*c*;*Col1a1*-YFP control ($n = 5$). Data presented as mean \pm SD normalized to control immune cells; one-way analysis of variance followed by Tukey multiple comparisons test. **, $P < 0.01$; ***, $P < 0.001$; ****, $P < 0.0001$. **B**, Flow cytometric analysis of the number of $ST2^+CD45^+$ immune cells in FVB/*n* normal lungs ($n = 5$) versus MMTV-PyMT metastases-bearing lungs ($n = 5$) and BALB/*c* normal lungs ($n = 7$) versus BALB/*c* mice bearing 4T1 tumor cell metastases following orthotopic injection ($n = 7$). Data presented as mean \pm SD; Welch *t* test. **, $P < 0.01$. **C**, Flow cytometry representative histogram of ST2 fluorescent intensity (MFI) out of total $CD45^+$ immune cells in normal lungs and metastases-bearing lungs (Mets). Histograms of Normal and Mets represent individual mice. FMO-fluorescent minus one. **D**, Quantification of flow cytometric analysis presented in **C**. Each sample was normalized to FMO control and to normal control. Welch *t* test, *, $P < 0.05$; ****, $P < 0.0001$. **E-H**, Flow cytometric analysis of ST2 fluorescence intensity in immune cell populations in normal lungs and metastases-bearing lungs derived from FVB/*n* normal lungs ($n = 3$) versus MMTV-PyMT metastases-bearing lungs ($n = 3$) and from BALB/*c* mice injected with 4T1 tumor cells ($n = 4$) or control BALB/*c* mice ($n = 4$). **E**, Lymphoid cells. **F**, Monocytes or macrophages. **G**, Granulocytes. **H**, Dendritic cells. Gating strategy presented in Supplementary Fig. S2C and S2D. Each cell population was normalized to FMO control and to normal control. Multiple *t* tests with Welch correction, FDR(Q) = 5%. *, $q < 0.05$; **, $q < 0.01$; ***, $q < 0.001$; ns, not significant.

Fibroblast-Derived IL33 Facilitates Lung Metastasis

**Figure 4.**

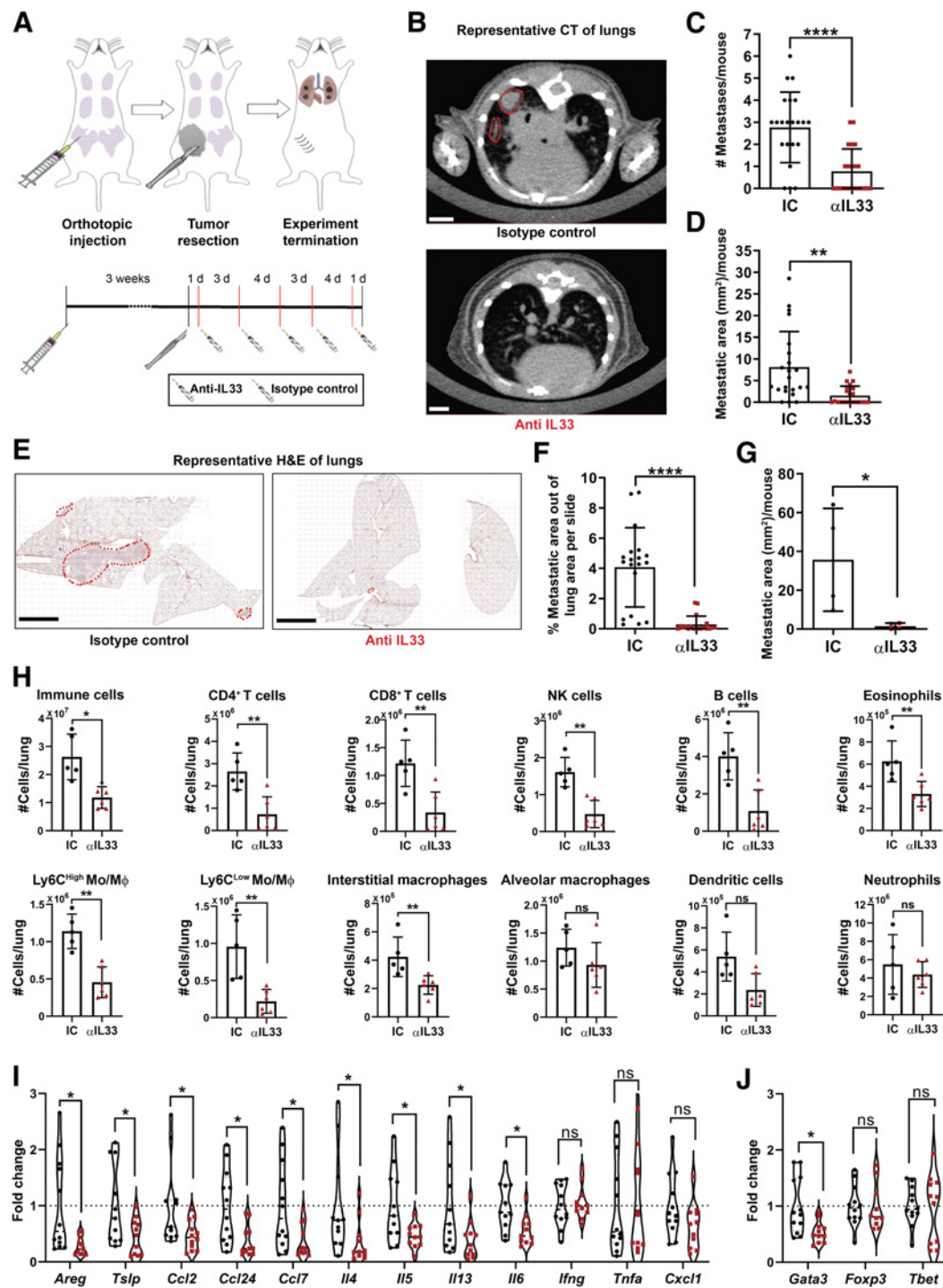
IL33 is functionally important for direct recruitment of T cells and eosinophils. **A**, Scheme for *in vitro* migration assays of neutrophil, monocyte, and T cells. BM-derived neutrophils and monocytes were isolated by gradient separation. CD3⁺ T cells were purified from spleen. **B–D**, Quantification of neutrophil (**B**), monocytes (**C**), and T cell (**D**) migration based on experimental design described in **A**. One-way ANOVA with Tukey correction for multiple comparisons tests. *, $P < 0.05$; **, $P < 0.01$; ***, $P < 0.001$; ****, $P < 0.0001$; ns, not significant. **E**, Scheme for eosinophil isolation and *in vitro* maturation, followed by migration assay. Eosinophil purity analysis is presented in Supplementary Fig. S3. **F**, Quantification of eosinophils migration. One-way ANOVA with Tukey correction for multiple comparisons tests. *, $P < 0.05$; **, $P < 0.01$.

expression in paired tumor and stromal samples from the same patient confirmed higher expression of *IL33* in the stroma (**Fig. 6B**). To test whether the expression of *IL33* changes with tumor progression, we compared its expression in epithelial and stromal cells derived from different tumor grades. Interestingly, *IL33* expression was significantly

upregulated in the stroma of higher-grade tumors (**Fig. 6C**), suggesting that stromal upregulation of *IL33* may be associated with tumor progression.

We further asked whether upregulation of *IL33* is characteristic of human breast cancer lung metastasis. To that end, we analyzed the

Shani et al.

**Figure 5.**

Inhibition of IL33 attenuates lung metastases and tempers type 2 immunity in the metastatic lung. **A**, Experimental design of IL33 inhibition *in vivo*. Experiments were performed five separate times with at least $n = 5$ mice per group. **B**, Representative CT scans of mice injected as described in **A**. Metastases are circled in red. Scale bars, 3 mm. IC, isotype control; α IL33, anti-IL33 antibody. **C**, Number of metastatic foci as identified by CT scans. Welch *t* test, ****, $P < 0.0001$. **D**, Area of metastases per mouse as measured by CT scans. Welch *t* test, **, $P < 0.01$. **E**, Representative H&E staining of lungs injected as described in **A**. Metastases are circled in red. Scale bars, 3 mm. **F**, Quantification of H&E staining for the metastatic area out of total lung area (metastatic burden). $n = 19$ lung tissue sections of four mice. Welch *t* test, ****, $P < 0.0001$. **G**, Quantification of H&E staining metastatic area per mouse. $n = 4$ mice. Welch one-tailed *t* test, *, $P < 0.05$. **H**, Flow cytometry immune cell populations analysis in mice injected as described in **A**. Multiple *t* tests with Welch correction, FDR(Q) = 1%. *, $q < 0.05$; **, $q < 0.01$; ****, $q < 0.0001$. **I** and **J**, Expression analysis by qRT-PCR of selected genes in lungs derived from mice injected with α IL33 or with IC, as described in **A**. $n \geq 11$ mice per group. Multiple *t* tests with Welch correction, FDR(Q) = 5%. *, $q < 0.05$; **, $q < 0.01$; ns, not significant.

Fibroblast-Derived IL33 Facilitates Lung Metastasis

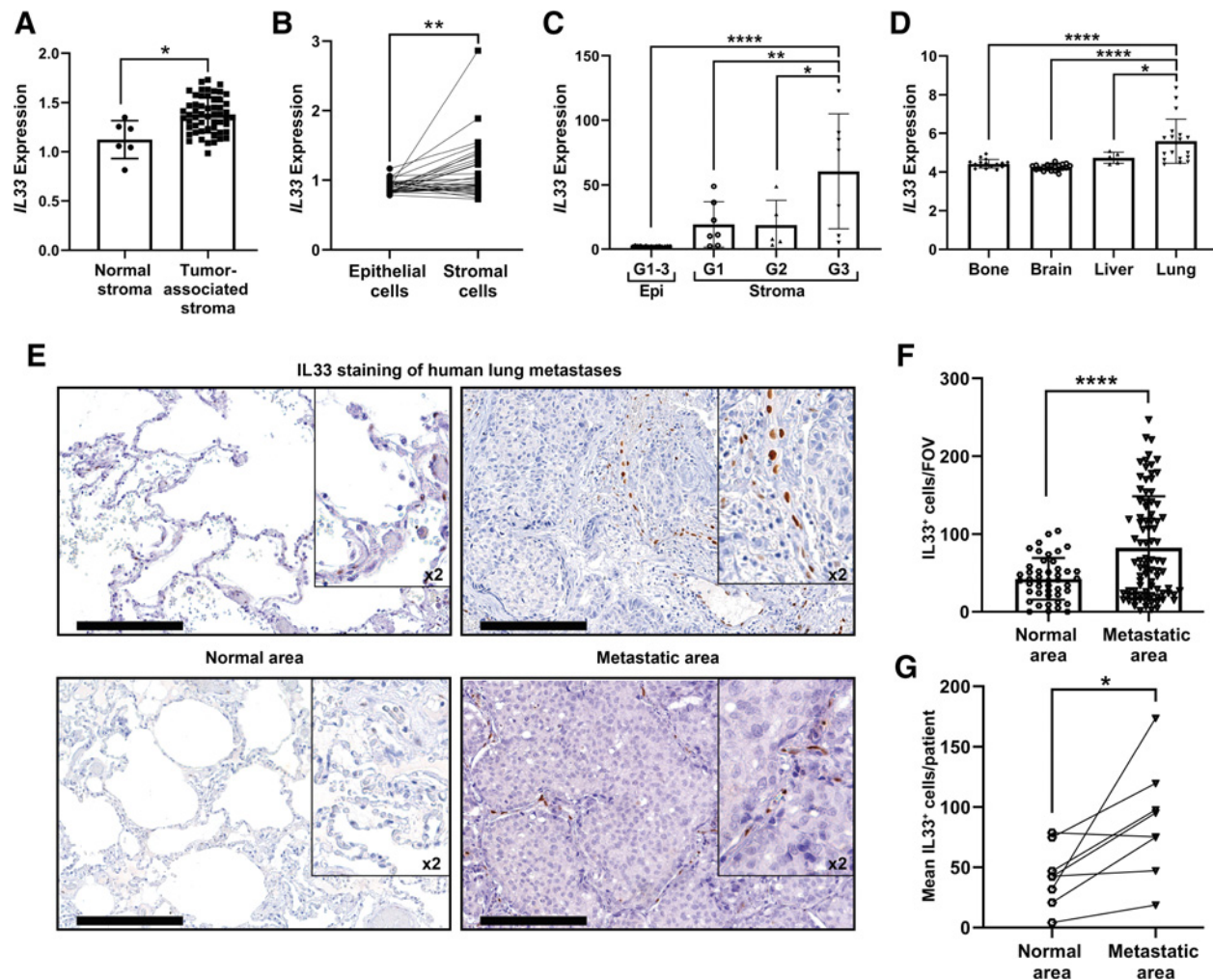


Figure 6.

IL33 is upregulated in the stroma of breast cancer primary tumors and lung metastases in human patients. **A**, IL33 expression in tumor-associated stroma as compared with normal stroma from GSE9014. Welch *t* test, *, $P < 0.05$. **B**, IL33 expression in paired patient samples of epithelial cells and tumor-associated stroma in primary breast tumors from GSE88715. Paired *t* test, **, $P < 0.01$. **C**, IL33 expression in primary breast-tumor tissue (Epi) and tumor associated-stroma (Stroma) from GSE14548. Stromal expression is divided into tumor grade (Stroma-grade 1, G1; Stroma-grade 2, G2; Stroma-grade 3, G3). For the epithelial expression of IL33, all grades were combined (G1-3). One-way ANOVA with Tukey correction for multiple comparisons, *, $P < 0.05$; **, $P < 0.01$; ****, $P < 0.0001$. **D**, IL33 mRNA expression in human breast cancer metastasis from different metastatic sites. Data were derived from GSE14020. One-way ANOVA with Tukey correction for multiple comparisons tests, *, $P < 0.05$; ****, $P < 0.0001$. **E**, Representative IHC staining of IL33 in lung metastases of patients with breast cancer ($n = 8$). Normal areas (remote from metastatic foci) were quantified as controls. Scale bars, 200 μm . **F**, Quantification of the number of IL33⁺ cells per FOV in IHC performed in **C**. 10–15 FOV/section. Data presented as mean \pm SD. Welch *t* test, ****, $P < 0.0001$. **G**, Analysis of the mean IL33⁺ cells/patient, compared with paired adjacent normal lung tissue. $n = 8$. Paired *t* test, *, $P < 0.05$.

expression of IL33 in a publicly available dataset of gene expression in the most common anatomic sites of breast cancer metastases: bone, brain, liver, and lungs (29, 30). Strikingly, the expression of IL33 was significantly higher in lung metastasis compared with other metastatic sites (Fig. 6D), suggesting a specific role for IL33 at the lung metastatic niche.

To further validate our findings, we performed histopathologic analysis in a cohort of patients with breast cancer with lung metastasis. IHC for IL33 in lung tissue sections revealed that IL33-expressing cells were highly increased in lung metastases, compared with normal lung tissue (Fig. 6E–G). Notably, the expression of IL33 in human lung metastases was limited to the stromal compartment, similarly to our observation in murine lung metastases. Thus, stromal IL33 is upre-

gulated in both human breast cancer primary tumors and lung metastases.

Discussion

In this study, we showed that IL33 is upregulated in MAFs in two different mouse models of spontaneous breast cancer metastasis to lungs—a transgenic model (MMTV-PyMT) and a transplantable model (4T1), following resection of the primary tumor. Moreover, analysis of lung metastases from patients with breast cancer revealed that stromal upregulation of IL33 is also operative in human disease. We further demonstrated that IL33 upregulation in the lung metastatic niche was associated with recruitment of immune cells and with

Shani et al.

modulating the cytokine and chemokine milieu in lungs toward type 2 inflammation. These changes were abrogated following inhibition of IL33. Importantly, targeting of IL33 *in vivo* by treating mice with neutralizing antibodies resulted in striking inhibition of lung metastasis, indicating a central role for fibroblast-derived IL33 in facilitating lung metastatic relapse, via modulating the metastatic immune microenvironment.

Our findings indicate that fibroblasts are the main source of IL33 in lung metastasis. Stromal cells were shown to modulate immunity and inflammation via IL33 in physiologic conditions (36, 37). In primary tumors, stromal-derived IL33 was implicated in tumor promotion by enhancing tumor cell growth and invasion (38, 39), and by affecting the recruitment and function of macrophages (40, 41). Our findings demonstrate that stromal-derived IL33 at the metastatic site facilitates metastasis by recruitment of multiple immune cells and by modulating the lung immune microenvironment. Interestingly, we previously showed that CAFs can function as sensors of damage-associated molecular patterns in breast tumors (21). Our current findings add another layer to this novel role of fibroblasts and show that tissue damage responses mediated by CAF secretion of the alarmin IL33 play an important role in facilitating metastasis.

By quantifying the alterations in cytokines and chemokines in lung metastasis, we found striking upregulation in the expression of multiple type 2 immunity mediators in lung metastasis, which was abolished when we inhibited IL33. Notably, IL33-associated changes in some TFs (Gata3, but not Tbet) suggested that IL33 may directly affect the expression of type 2 immunity-related factors. Moreover, we analyzed the immune cell milieu in lung metastasis and found a prominent increase in multiple immune cell populations including eosinophils, T cells and inflammatory monocytes. Indeed, we found that immune cell infiltration was abolished when IL33 was inhibited *in vivo*, suggesting a central role for stromal-derived IL33 in recruitment of these cell types. IL33 was previously implicated in affecting eosinophil recruitment and maturation (42), as well as recruitment and reprogramming of macrophages and dendritic cells toward an immunosuppressive function in primary tumors (43). We showed that this is also operative in metastasis. Interestingly, while eosinophil recruitment was IL33 dependent, their ablation was not sufficient to inhibit lung metastasis, suggesting that the role of IL33 in promoting metastasis is not restricted to a single downstream cell type. Thus, by performing a comprehensive analysis of the immune milieu at the metastatic microenvironment, followed by functional *in vivo* experiments, our findings add a new dimension to the formation of a hospitable metastatic niche by revealing a central role for CAF-derived IL33 in mediating the recruitment of multiple immune cell types to lung metastasis, and by driving type 2 inflammation.

IL33 has a controversial role in cancer, with studies showing tumor-promoting or tumor-inhibitory functions in various cancer types (44, 45). Notably, a protective role for IL33 was mostly demonstrated in studies in which IL33 was exogenously administered or overexpressed in tumor cells (46–48), indicating that the source of IL33

and the physiologic context are of critical importance to its function. Moreover, studies showing tumor-promoting roles for IL33 mostly focused on primary tumor growth. Our study demonstrates for the first time in a clinically relevant model of spontaneous lung metastasis, following surgical resection of the primary tumor, that fibroblast-derived IL33 plays a functional role in the lung metastatic niche.

Notably, our analysis of IL33 expression in human breast cancer metastasis indicated that upregulation of IL33 is specific for lung metastases. Taken together with our results in mouse models, these findings suggest that targeting IL33 may be beneficial for inhibiting lung metastatic relapse of breast cancer. Targeting of IL33 was tested for the treatment of asthma, chronic obstructive pulmonary disease and peanut allergy (49). Interestingly, allergen-induced pulmonary inflammation was shown to enhance lung colonization by circulating tumor cells in a mouse model of experimental metastasis. Moreover, analysis of a clinical breast cancer database revealed higher incidence of lung metastasis in asthmatic patients as compared with nonasthmatic patients (50). Thus, adjuvant targeting of IL33, limiting pulmonary inflammation, may be beneficial for patients with breast cancer with preexisting pulmonary disease.

In summary, our study reveals a novel interaction axis between fibroblasts and immune cells in the lung metastatic microenvironment, mediated via CAF-derived IL33 that establishes a hospitable inflammatory niche, by driving type 2 inflammation. Our findings suggest that targeting the IL33 pathway may offer therapeutic benefit to prevent or treat lung metastasis.

Disclosure of Potential Conflicts of Interest

No potential conflicts of interest were disclosed.

Authors' Contributions

O. Shani: Conceptualization, formal analysis, investigation, methodology, writing-original draft. **T. Vorobyov:** Investigation. **L. Monteran:** Investigation. **D. Lavie:** Investigation. **N. Cohen:** Investigation. **Y. Raz:** Investigation. **G. Tsarfaty:** Formal analysis. **C. Avivi:** Investigation. **I. Barshack:** Resources. **N. Erez:** Conceptualization, supervision, methodology, writing-original draft, project administration.

Acknowledgments

This research was supported by grants to N. Erez from the European Research Council (ERC) under the European Union's Horizon 2020 Research and Innovation Programme (grant agreement No. 637069 MetCAF), from the Israel Science Foundation (#1060/18), the Emerson Collective, and the Israel Cancer Research Fund (ICRF Project Grant). The authors would like to thank Sharon Grisaru for her assistance with staining of eosinophils and Ariel Munitz for critical reading and useful discussion of the manuscript.

The costs of publication of this article were defrayed in part by the payment of page charges. This article must therefore be hereby marked *advertisement* in accordance with 18 U.S.C. Section 1734 solely to indicate this fact.

Received June 22, 2020; revised August 26, 2020; accepted September 29, 2020; published first October 6, 2020.

References

1. Quail DF, Joyce JA. Microenvironmental regulation of tumor progression and metastasis. *Nat Med* 2013;19:1423–37.
2. Peinado H, Zhang H, Matei IR, Costa-Silva B, Hoshino A, Rodrigues G, et al. Pre-metastatic niches: organ-specific homes for metastases. *Nat Rev Cancer* 2017;17:302–17.
3. Albrengus J, Shields MA, Ng D, Park CG, Ambrico A, Poindexter ME, et al. Neutrophil extracellular traps produced during inflammation awaken dormant cancer cells in mice. *Science* 2018;361:eao4227.
4. Coffelt SB, Kersten K, Doornebal CW, Weiden J, Vrijland K, Hau CS, et al. IL-17-producing gammadelta T cells and neutrophils conspire to promote breast cancer metastasis. *Nature* 2015;522:345–8.
5. DeNardo DG, Barreto JB, Andreu P, Vasquez L, Tawfik D, Kolhatkar N, et al. CD4(+) T cells regulate pulmonary metastasis of mammary carcinomas by enhancing protumor properties of macrophages. *Cancer Cell* 2009;16:91–102.
6. Fridlender ZG, Albelda SM, Granot Z. Promoting metastasis: neutrophils and T cells join forces. *Cell Res* 2015;25:765–6.

Fibroblast-Derived IL33 Facilitates Lung Metastasis

7. Kobayashi M, Kobayashi H, Pollard RB, Suzuki F. A pathogenic role of Th2 cells and their cytokine products on the pulmonary metastasis of murine B16 melanoma. *J Immunol* 1998;160:5869–73.
8. Zhang Q, Qin J, Zhong L, Gong L, Zhang B, Zhang Y, et al. CCL5-mediated Th2 immune polarization promotes metastasis in luminal breast cancer. *Cancer Res* 2015;75:4312–21.
9. Schmitz J, Owyang A, Oldham E, Song Y, Murphy E, McClanahan TK, et al. IL-33, an interleukin-1-like cytokine that signals via the IL-1 receptor-related protein ST2 and induces T helper type 2-associated cytokines. *Immunity* 2005;23:479–90.
10. Mantovani A, Dinarello CA, Molgora M, Garlanda C. Interleukin-1 and related cytokines in the regulation of inflammation and immunity. *Immunity* 2019;50:778–95.
11. Rider P, Voronov E, Dinarello CA, Apte RN, Cohen I. Alarmins: feel the stress. *J Immunol* 2017;198:1395–402.
12. Moussion C, Ortega N, Girard JP. The IL-1-like cytokine IL-33 is constitutively expressed in the nucleus of endothelial cells and epithelial cells *in vivo*: a novel 'alarmin'? *PLoS One* 2008;3:e3331.
13. Pichery M, Mirey E, Mercier P, Lefrancais E, Dujardin A, Ortega N, et al. Endogenous IL-33 is highly expressed in mouse epithelial barrier tissues, lymphoid organs, brain, embryos, and inflamed tissues: *in situ* analysis using a novel IL-33-LacZ gene trap reporter strain. *J Immunol* 2012;188:3488–95.
14. Liew FY, Girard JP, Turnquist HR. Interleukin-33 in health and disease. *Nat Rev Immunol* 2016;16:676–89.
15. Cayrol C, Girard JP. IL-33: an alarmin cytokine with crucial roles in innate immunity, inflammation and allergy. *Curr Opin Immunol* 2014;31:31–7.
16. Drake LY, Kita H. IL-33: biological properties, functions, and roles in airway disease. *Immunol Rev* 2017;278:173–84.
17. Shen JX, Liu J, Zhang GJ. Interleukin-33 in malignancies: friends or foes? *Front Immunol* 2018;9:3051.
18. Liu L, Liu L, Yao HH, Zhu ZQ, Ning ZL, Huang Q. Stromal myofibroblasts are associated with poor prognosis in solid cancers: a meta-analysis of published studies. *PLoS One* 2016;11:e0159947.
19. Cohen N, Shani O, Raz Y, Sharon Y, Hoffman D, Abramovitz L, et al. Fibroblasts drive an immunosuppressive and growth-promoting microenvironment in breast cancer via secretion of Chitinase 3-like 1. *Oncogene* 2017;36:4457–68.
20. Erez N, Truitt M, Olson P, Arron ST, Hanahan D. Cancer-associated fibroblasts are activated in incipient neoplasia to orchestrate tumor-promoting inflammation in an NF-kappaB-dependent manner. *Cancer Cell* 2010;17:135–47.
21. Ershaid N, Sharon Y, Doron H, Raz Y, Shani O, Cohen N, et al. NLRP3 inflammasome in fibroblasts links tissue damage with inflammation in breast cancer progression and metastasis. *Nat Commun* 2019;10:4375.
22. Raz Y, Cohen N, Shani O, Bell RE, Novitskiy SV, Abramovitz L, et al. Bone marrow-derived fibroblasts are a functionally distinct stromal cell population in breast cancer. *J Exp Med* 2018;215:3075–93.
23. Shani O, Raz Y, Megides O, Shacham H, Cohen N, Silverbush D, et al. Evolution of metastases-associated fibroblasts in the lung microenvironment is driven by stage-specific transcriptional plasticity. *bioRxiv* 2019. DOI: <https://doi.org/10.1101/778936>.
24. Misharin AV, Morales-Nebreda L, Mutlu GM, Budinger GR, Perlman H. Flow cytometric analysis of macrophages and dendritic cell subsets in the mouse lung. *Am J Respir Cell Mol Biol* 2013;49:503–10.
25. Yu YR, O'Koren EG, Hotten DF, Kan MJ, Kopin D, Nelson ER, et al. A protocol for the comprehensive flow cytometric analysis of immune cells in normal and inflamed murine non-lymphoid tissues. *PLoS One* 2016;11:e0150606.
26. Ma XJ, Dahiya S, Richardson E, Erlander M, Sgroi DC. Gene expression profiling of the tumor microenvironment during breast cancer progression. *Breast Cancer Res* 2009;11:R7.
27. Finak G, Bertos N, Pepin F, Sadekova S, Souleimanova M, Zhao H, et al. Stromal gene expression predicts clinical outcome in breast cancer. *Nat Med* 2008;14:518–27.
28. Gruosso T, Tigoux M, Manem VSK, Bertos N, Zuo D, Perlich I, et al. Spatially distinct tumor immune microenvironments stratify triple-negative breast cancers. *J Clin Invest* 2019;129:1785–800.
29. Xu J, Acharya S, Sahin O, Zhang Q, Saito Y, Yao J, et al. 14-3-3zeta turns TGF-beta's function from tumor suppressor to metastasis promoter in breast cancer by contextual changes of Smad partners from p53 to Gli2. *Cancer Cell* 2015;27:177–92.
30. Zhang XH, Wang Q, Gerald W, Hudis CA, Norton L, Smid M, et al. Latent bone metastasis in breast cancer tied to Src-dependent survival signals. *Cancer Cell* 2009;16:67–78.
31. Jovanovic IP, Pejnovic NN, Radosavljevic GD, Pantic JM, Milovanovic MZ, Arsenijevic NN, et al. Interleukin-33/ST2 axis promotes breast cancer growth and metastases by facilitating intratumoral accumulation of immunosuppressive and innate lymphoid cells. *Int J Cancer* 2014;134:1669–82.
32. Li J, Liu C, Chen Y, Gao C, Wang M, Ma X, et al. Tumor characterization in breast cancer identifies immune-relevant gene signatures associated with prognosis. *Front Genet* 2019;10:1119.
33. Martin NT, Martin MU. Interleukin 33 is a guardian of barriers and a local alarmin. *Nat Immunol* 2016;17:122–31.
34. Pinto SM, Subbannayya Y, Rex DAB, Raju R, Chatterjee O, Advani J, et al. A network map of IL-33 signaling pathway. *J Cell Commun Signal* 2018;12:615–24.
35. De la Fuente M, MacDonald TT, Hermoso MA. The IL-33/ST2 axis: role in health and disease. *Cytokine Growth Factor Rev* 2015;26:615–23.
36. Dahlgren MW, Jones SW, Cautivo KM, Dubinin A, Ortiz-Carpena JF, Farhat S, et al. Adventitial stromal cells define group 2 innate lymphoid cell tissue niches. *Immunity* 2019;50:707–22.e6.
37. Mahlakoiv T, Flamar AL, Johnston LK, Moriyama S, Putzel GG, Bryce PJ, et al. Stromal cells maintain immune cell homeostasis in adipose tissue via production of interleukin-33. *Sci Immunol* 2019;4:eaax0416.
38. Chen SF, Nieh S, Jao SW, Wu MZ, Liu CL, Chang YC, et al. The paracrine effect of cancer-associated fibroblast-induced interleukin-33 regulates the invasiveness of head and neck squamous cell carcinoma. *J Pathol* 2013;231:180–9.
39. Zhou Q, Wu X, Wang X, Yu Z, Pan T, Li Z, et al. The reciprocal interaction between tumor cells and activated fibroblasts mediated by TNF-alpha/IL-33/ST2L signaling promotes gastric cancer metastasis. *Oncogene* 2020;39:1414–28.
40. Andersson P, Yang Y, Hosaka K, Zhang Y, Fischer C, Braun H, et al. Molecular mechanisms of IL-33-mediated stromal interactions in cancer metastasis. *JCI Insight* 2018;3:e122375.
41. Yang Y, Andersson P, Hosaka K, Zhang Y, Cao R, Iwamoto H, et al. The PDGF-BB-SOX7 axis-modulated IL-33 in pericytes and stromal cells promotes metastasis through tumour-associated macrophages. *Nat Commun* 2016;7:11385.
42. Johnston LK, Hsu CL, Krier-Burris RA, Chhibba KD, Chien KB, McKenzie A, et al. IL-33 precedes IL-5 in regulating eosinophil commitment and is required for eosinophil homeostasis. *J Immunol* 2016;197:3445–53.
43. Afferni C, Buccione C, Andreone S, Galdiero MR, Varricchi G, Marone G, et al. The pleiotropic immunomodulatory functions of IL-33 and its implications in tumor immunity. *Front Immunol* 2018;9:2601.
44. Baker KJ, Houston A, Brint E. IL-1 family members in cancer; two sides to every story. *Front Immunol* 2019;10:1197.
45. Fournie JJ, Poupot M. The pro-tumorigenic IL-33 involved in antitumor immunity: a Yin and Yang cytokine. *Front Immunol* 2018;9:2506.
46. Jin Z, Lei L, Lin D, Liu Y, Song Y, Gong H, et al. IL-33 released in the liver inhibits tumor growth via promotion of CD4(+) and CD8(+) T cell responses in hepatocellular carcinoma. *J Immunol* 2018;201:3770–9.
47. Dominguez D, Ye C, Geng Z, Chen S, Fan J, Qin L, et al. Exogenous IL-33 restores dendritic cell activation and maturation in established cancer. *J Immunol* 2017;198:1365–75.
48. Qi L, Zhang Q, Miao Y, Kang W, Tian Z, Xu D, et al. Interleukin-33 activates and recruits natural killer cells to inhibit pulmonary metastatic cancer development. *Int J Cancer* 2020;146:1421–34.
49. Lawrence MG, Steinke JW, Borish L. Cytokine-targeting biologics for allergic diseases. *Ann Allergy Asthma Immunol* 2018;120:376–81.
50. Taranova AG, Maldonado D 3rd, Vachon CM, Jacobsen EA, Abdala-Valencia H, McGarry MP, et al. Allergic pulmonary inflammation promotes the recruitment of circulating tumor cells to the lung. *Cancer Res* 2008;68:8582–9.

Cancer Research

The Journal of Cancer Research (1916–1930) | The American Journal of Cancer (1931–1940)

Fibroblast-Derived IL33 Facilitates Breast Cancer Metastasis by Modifying the Immune Microenvironment and Driving Type 2 Immunity

Ophir Shani, Tatiana Vorobyov, Lea Monteran, et al.

Cancer Res 2020;80:5317-5329. Published OnlineFirst October 6, 2020.

Updated version Access the most recent version of this article at:
doi:[10.1158/0008-5472.CAN-20-2116](https://doi.org/10.1158/0008-5472.CAN-20-2116)

Supplementary Material Access the most recent supplemental material at:
<http://cancerres.aacrjournals.org/content/suppl/2020/10/06/0008-5472.CAN-20-2116.DC1>

Cited articles This article cites 49 articles, 11 of which you can access for free at:
<http://cancerres.aacrjournals.org/content/80/23/5317.full#ref-list-1>

E-mail alerts [Sign up to receive free email-alerts](#) related to this article or journal.

Reprints and Subscriptions To order reprints of this article or to subscribe to the journal, contact the AACR Publications Department at pubs@aacr.org.

Permissions To request permission to re-use all or part of this article, use this link
<http://cancerres.aacrjournals.org/content/80/23/5317>.
Click on "Request Permissions" which will take you to the Copyright Clearance Center's (CCC) Rightslink site.